

**Quartz textures, trace elements, fluid inclusions, and in-situ oxygen isotopes from
Aktogai porphyry Cu deposit, Kazakhstan**

**Changhao Li ^{1,3}, Ping Shen ^{1,2,3*}, Reimar Seltmann ⁴, Di Zhang ^{5,2}, Hongdi Pan ⁶,
Eleonora Seitmuratova ⁷**

¹Key Laboratory of Mineral Resources, Institute of Geology and Geophysics, Chinese
Academy of Sciences, Beijing 100029, China;

²University of Chinese Academy of Sciences, Beijing 100049, China;

³Institutions of Earth Science, Chinese Academy of Sciences, Beijing 100029, China;

⁴Center for Russian and Central EurAsian Mineral Studies, Natural History Museum,
London SW7 5BD, UK

⁵State Key Laboratory of Lithospheric Evolution, Institute of Geology and Geophysics,
Chinese Academy of Sciences, Beijing 100029, China

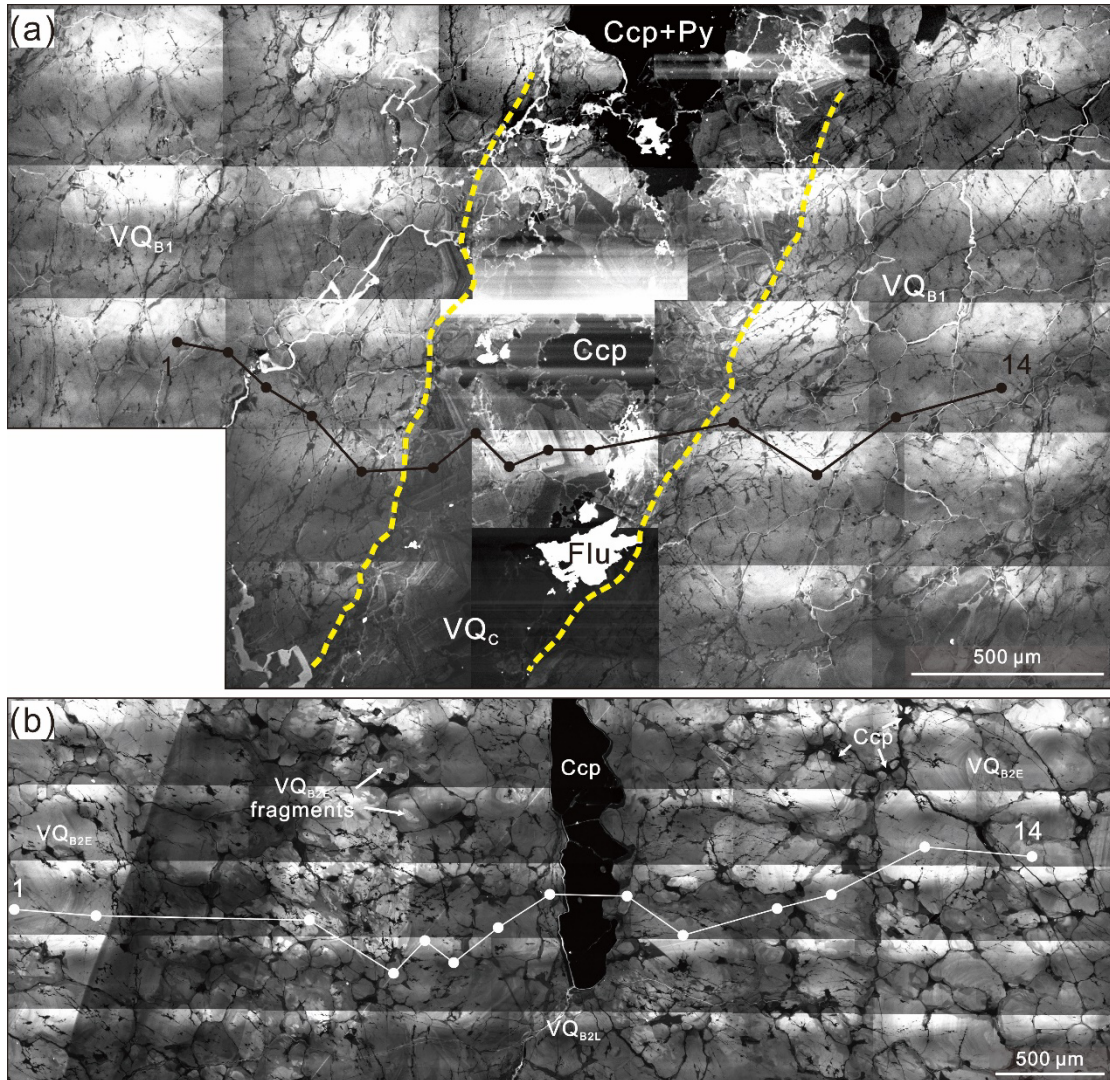
⁶College of Earth Sciences, Chang'an University, Xi'an 710054, China

⁷Laboratory of Geological Formations, K. Satpaev Institute of Geological Sciences,
Almaty 050010, Kazakhstan

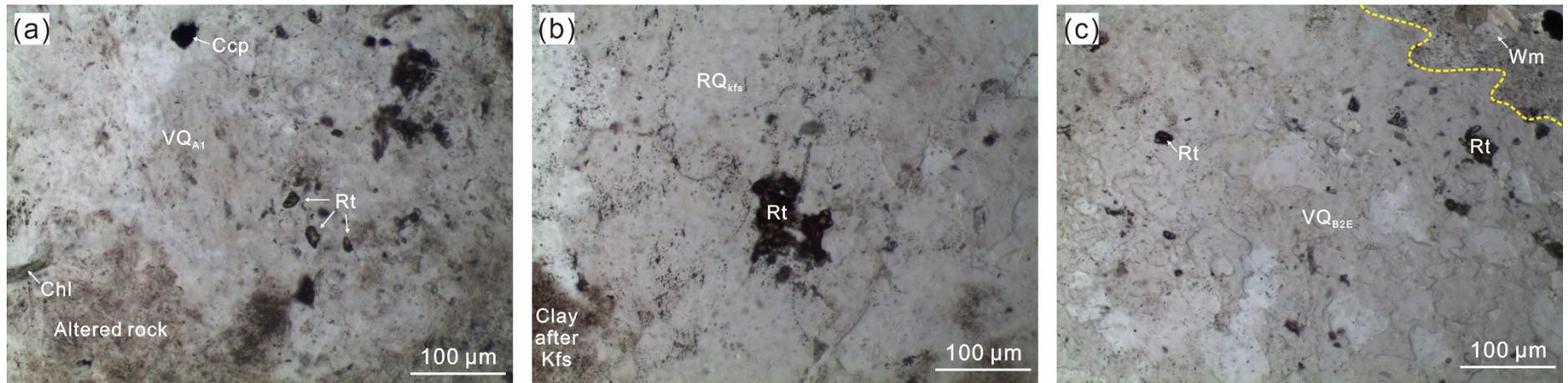
Corresponding author:

Name: Ping Shen

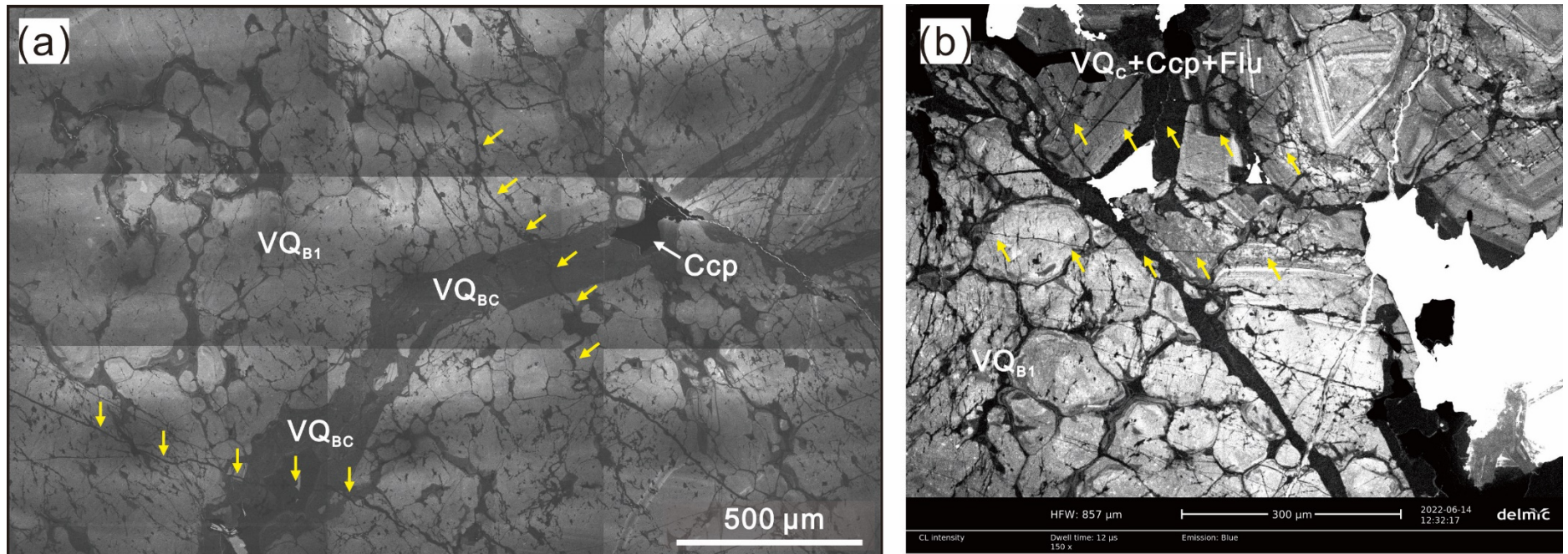
E-mail: pshen@mail.iggcas.ac.cn



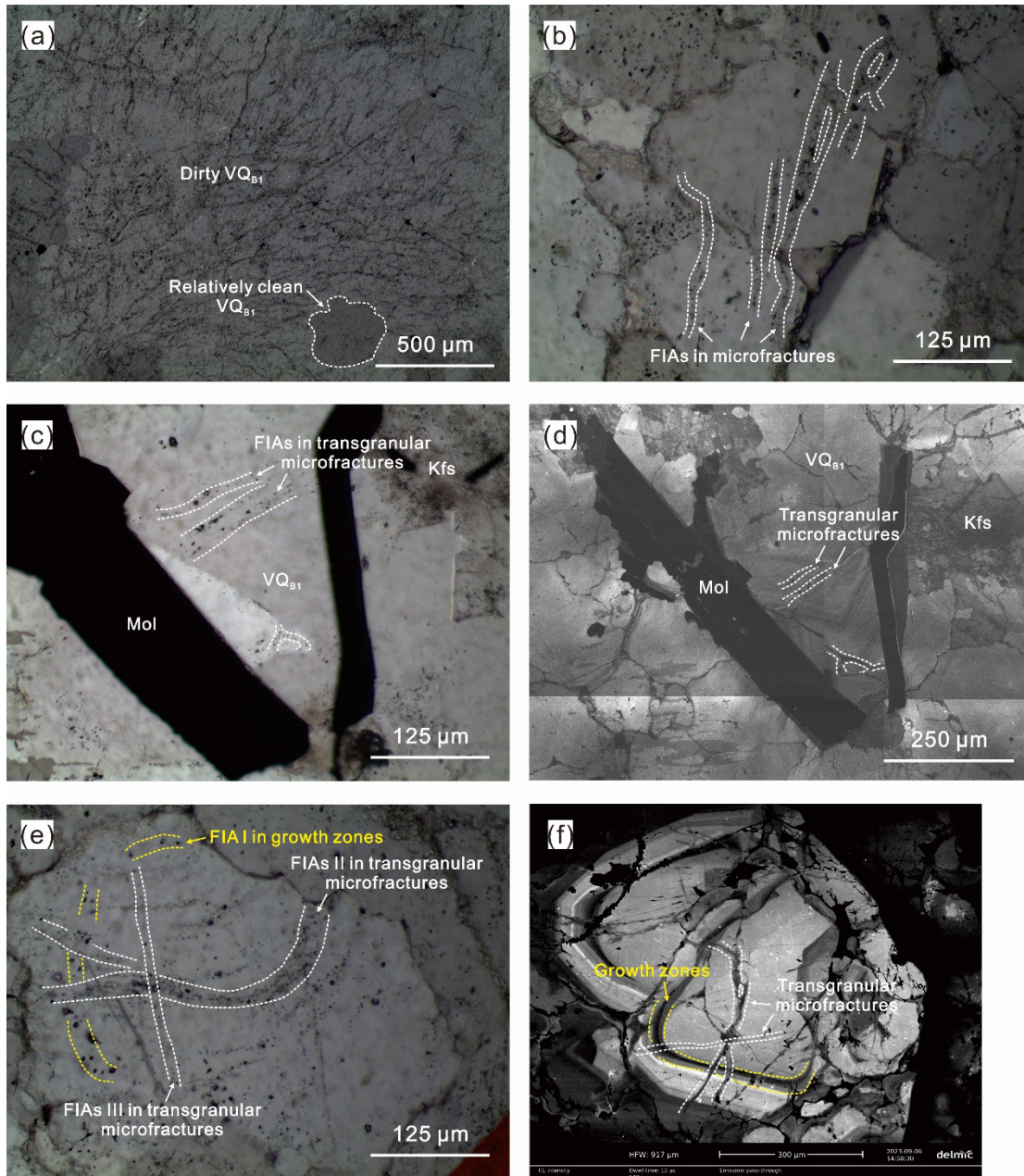
ESM Fig. 2 (a) CL images showed VQC in a quartz-chalcopyrite-pyrite-epidote-chlorite vein (C vein) crosscut VQB1 grains. Yellow dashed lines show the edge of the C vein. (b) CL images of a quartz-chalcopyrite-pyrite vein (B2 vein).



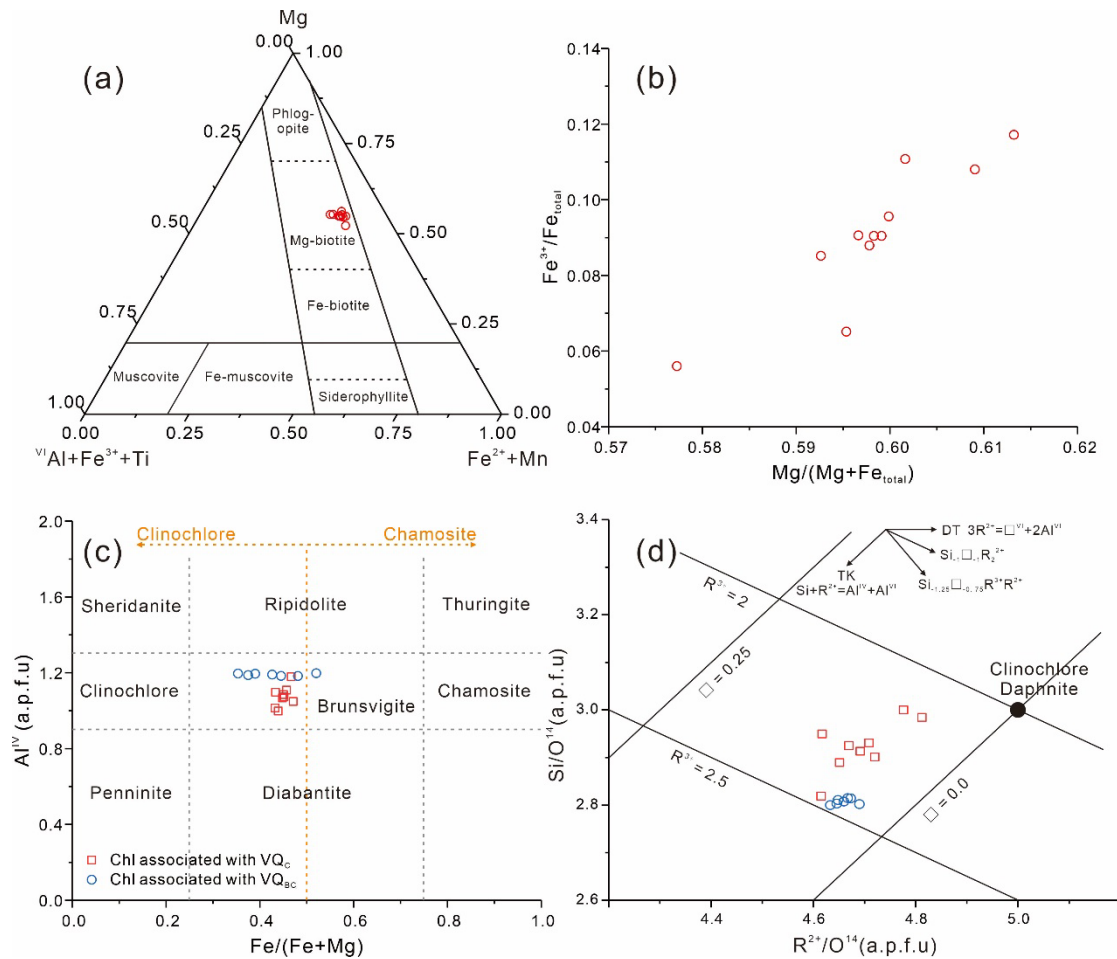
ESM Fig. 3 Rutile grains precipitated in (a) a discontinuous quartz vein (A1 vein), (b) K-feldspar altered rocks, and (c) a quartz-chalcopyrite-
pyrite vein with thin K-feldspar halos (B2 vein). Yellow dashed lines show the margin of the vein.



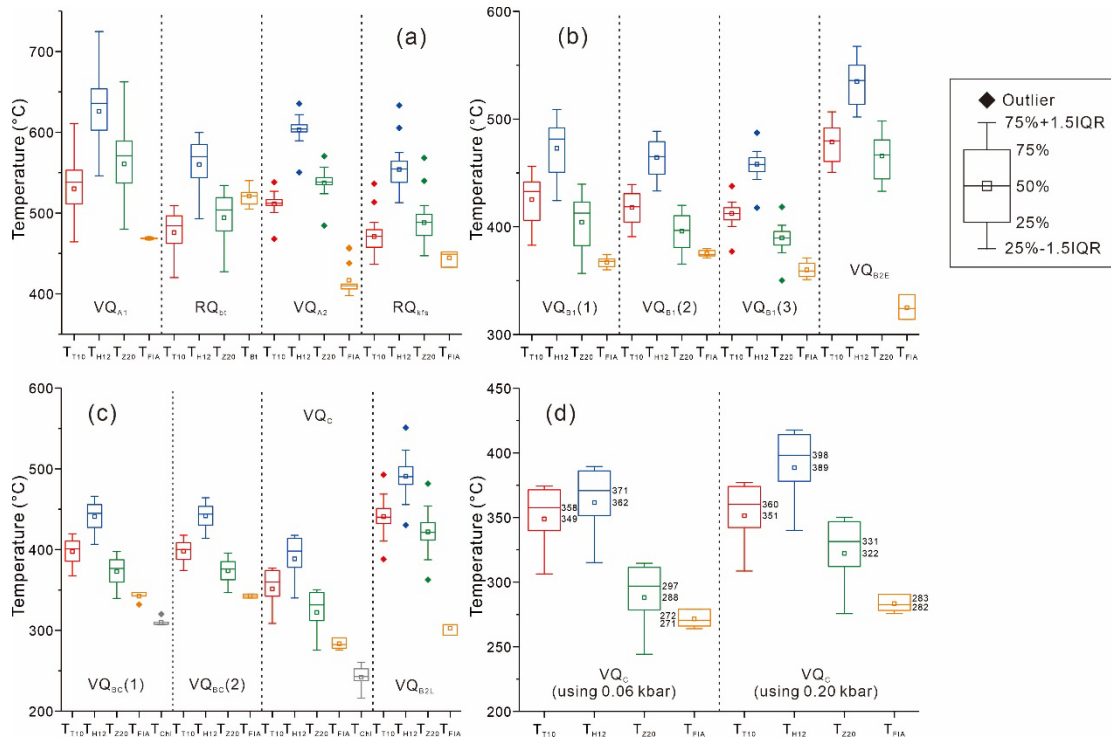
ESM Fig. 4 Yellow arrows show the latest quartz with the blackest CL color crosscut VQ_{BC} and VQ_C .



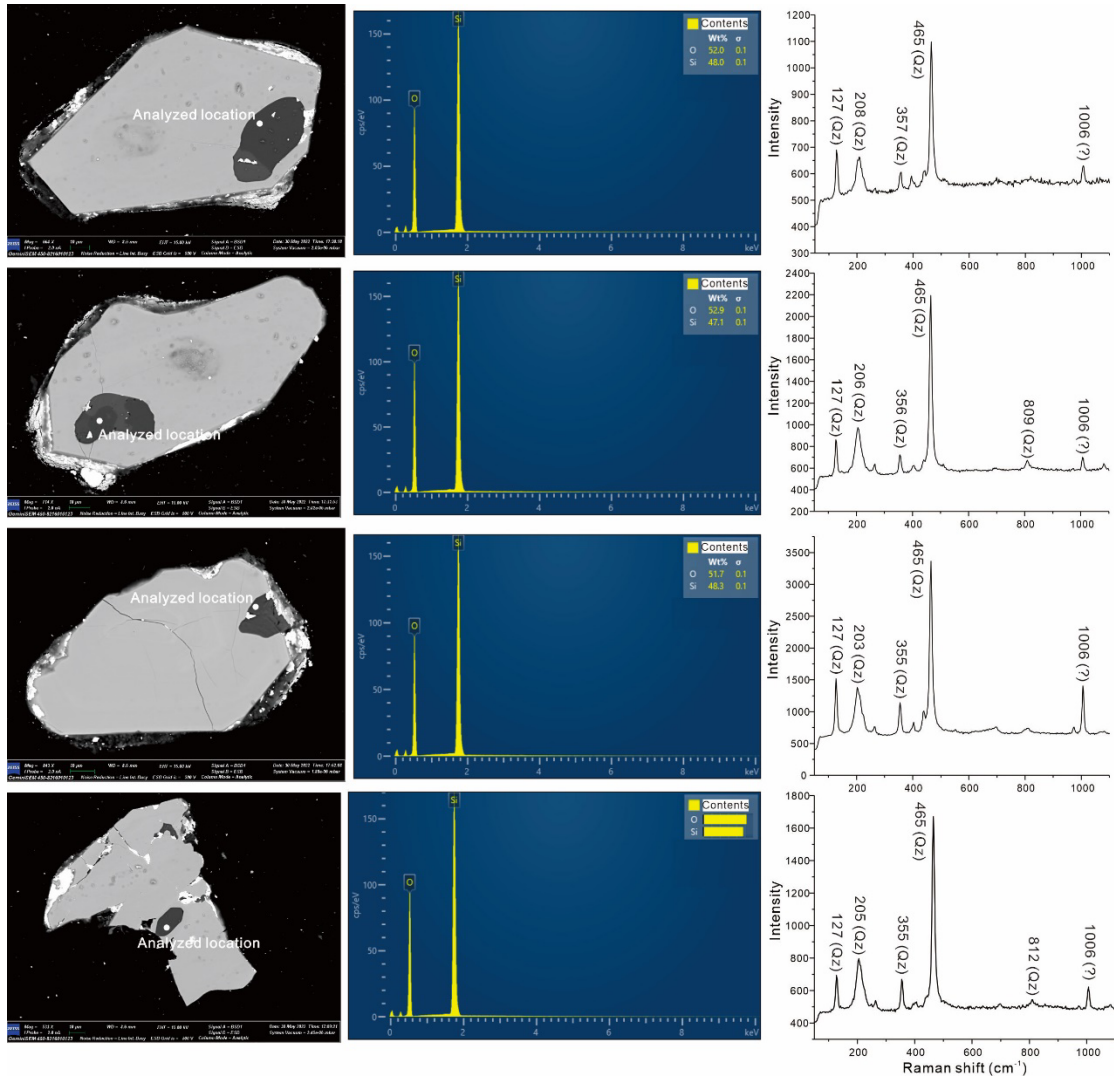
ESM Fig. 5 (a) In one vein, the fluid inclusions that were used for analysis were located on relatively clean quartz grains, and quartz grains containing a complex genesis of fluid inclusions (dirty quartz) were discarded. (b) FIAs in transgranular microfractures crosscut quartz grain boundaries. (c-d) CL images showed FIAs in transgranular microfractures crosscut VQ_{B1} grains. (e-f) CL images identified the multi-stage FIAs in one quartz grain.



ESM Fig. 6 (a) $(Fe^{2+}+Mn)$ - Mg - $(^{VI}Al+Fe^{3+}+Ti)$ (a.p.f.u) diagram of biotite (modified from Foster 1960). (b) $Mg/(Mg+Fe_{total})$ vs. Fe^{3+}/Fe_{total} (a.p.f.u) diagram of biotite. (c) $Fe/(Fe+Mg)$ vs. Al^{VI} (a.p.f.u) diagram of chlorite (modified from Arbiol et al. 2021). (d) R^{2+} ($= Fe^{2+}+Mg^{2+}$) (a.p.f.u) vs. Si (a.p.f.u) diagram of chlorite. R^{3+} and \square refer to trivalent cations (Al^{3+} and Fe^{3+}) and vacancies, respectively.



ESM Fig. 7 (a-c) Comparison of the formation temperatures obtained by different Ti-in-quartz thermometers. The formation temperatures of biotite, chlorite, and fluid inclusions are also shown. (1), (2), and (3) represent the quartz-K-feldspar-molybdenite-rutile, quartz-K-feldspar-molybdenite, and quartz-chalcopyrite-K-feldspar veins, respectively. **(d)** This plot shows that pressure has little effect on the discrepancy between the results of fluid inclusion microthermometry and Ti-in-quartz thermometer. This is because (1) the same pressures were used for the different estimation methods; (2) the Aktogai deposit formed under low-pressure conditions, and the pressure had little effect on the estimation results (generally <math><30\text{ }^\circ\text{C}</math>); (3) the two methods mentioned above are affected by the pressure to similar extents, and the discrepancy is similar under different pressure conditions.



ESM Fig. 8 Quartz occurred as mineral inclusions in the zircon. The high-brightness BSE image is unpolished gold (plated when performing SIMS experiments).

References cited in Electronic Supplementary Material

- Arbiol, C., Layne, G.D., Zannoni, G., and Šegvić, B. (2021) Characteristics and genesis of phyllosilicate hydrothermal assemblages from Neoproterozoic epithermal Au-Ag mineralization of the Avalon Zone of Newfoundland, Canada. *Applied Clay Science*, 202, 105960.
- Foster, M.D. (1960) Interpretation of the composition of trioctahedral micas. *US Geol Surv Prof Pap*, 354-B, 11-49.
- Huang, R.F., and Audétat, A. (2012) The titanium-in-quartz (TitaniQ) thermobarometer: a critical examination and re-calibration. *Geochimica et Cosmochimica Acta*, 84, 75-89.
- Thomas, J.B., Watson, E.B., Spear, F.S., Shemella, P.T., Nayak, S.K., and Lanzirrotti, A. (2010) TitaniQ under pressure: the effect of pressure and temperature on the solubility of Ti in quartz. *Contributions to Mineralogy and Petrology*, 160, 743-759.
- Zhang, C., Li, X., Almeev, R.R., Horn, I., Behrens, H., and Holtz, F. (2020) Ti-in-quartz thermobarometry and TiO₂ solubility in rhyolitic melts: new experiments and parametrization. *Earth and Planetary Science Letters*, 538, 116213.